Mon. Not. R. Astron. Soc. **307,** 279–292 (1999)

A class of exact MHD models for astrophysical jets

N. Vlahakis[1⋆] and K. Tsinganos[1,2⋆]
[1]*Department of Physics, University of Crete, GR-710 03 Heraklion, Crete, Greece*
[2]*Foundation for Research and Technology Hellas (FORTH), GR-711 10 Heraklion, Crete, Greece*

Accepted 1999 February 4. Received 1998 December 30; in original form 1998 July 27

ABSTRACT

This paper examines a new class of exact and self-consistent MHD solutions that describe steady and axisymmetric hydromagnetic outflows from the atmosphere of a magnetized and rotating central object with possibly an orbiting accretion disc. The plasma is driven against gravity by a thermal pressure gradient, as well as by magnetic rotator and radiative forces. At the Alfvénic and fast critical points the appropriate criticality conditions are applied. The outflow starts almost radially, but after the Alfvén transition and before the fast critical surface is encountered, the magnetic pinching force bends the poloidal streamlines into a cylindrical jet-type shape. The terminal speed, Alfvén number and cross-sectional area of the jet, as well as its final pressure and density, obtain uniform values at large distances from the source. The goal of the study is to give an analytical discussion of the two-dimensional interplay of the thermal pressure gradient, gravitational, Lorentz and inertial forces in accelerating and collimating an MHD flow. A parametric study of the model is also given, as well as a brief sketch of its applicability to a self-consistent modelling of collimated outflows from various astrophysical objects. The analysed model succeeds in giving for the first time an exact MHD solution for jet-type outflows extending from the stellar surface to infinity where the outflow can be superfast, in agreement with the MHD causality principle.

Key words: MHD – plasmas – stars: atmospheres – stars: mass-loss – ISM: jets and outflows – galaxies: jets.

1 INTRODUCTION

Collimated outflows are quite common in astrophysics and cosmic jets are observed in the radio, infrared, optical, UV and X-ray parts of the spectrum, from the ground and space, most recently via the *Hubble Space Telescope*. Thus, classes of objects in association with which jets are observed include young stellar objects (YSOs) (Ray 1996), old mass-losing stars and planetary nebulae (Livio 1997), black hole X-ray transients (Mirabel & Rodriguez 1996), supersoft X-ray sources (Kahabka & Trumper 1996), high-mass X-ray binaries, cataclysmic variables (Shahbaz et al. 1997) and many active galactic nuclei (AGN) and quasars (Biretta 1996; Ferrari et al. 1996). However, despite their observed abundance, several key questions on their acceleration and collimation, among others, have not yet been resolved.

The theoretical magnetohydrodynamic (MHD) modelling of jets is not a simple undertaking, basically because of the fact that the set of MHD equations is highly non-linear with singular or critical surfaces appearing in their domain of solutions; these singularities – through which a physical solution inevitably will have to pass – are not known a priori but they are instead determined simultaneously with the complete solution. The purpose of the present study is to construct systematically a self-consistent MHD model for astrophysical jets from the stellar base to infinity where the interplay of the various forces acting on the plasma, which are able to accelerate and collimate the outflow, is analytically examined. This modelling is an improvement on the very few existing models developed so far with the same goal. For example, it is fully two-dimensional (cf. the models of Parker 1958 and Weber & Davis 1967 which are 1D), it does not contain singularities along the symmetry axis and the outflow is not over-focused but extends to large distances (e.g. the models of Blandford & Payne 1982 and Ostriker 1997 do contain such singularities), the equation of state is not constrained by the artificial polytropic assumption (as e.g. in the polytropic analysis of Contopoulos & Lovelace 1994; Heyvaerts & Norman 1989), the thermal pressure is meridionally anisotropic (cf. the model with a meridionally isotropic pressure in Sauty & Tsinganos 1994), the shape of the jet is self-consistently determined and not a priori given (e.g. the models in Cao & Spruit 1994, Kudoh & Shibata 1997 and Trussoni, Tsinganos & Sauty 1997 have an a priori given field line shape), there is a steady asymptotic state (cf. Uchida & Shibata 1985; Ouyed & Pudritz 1997a,b; Goodson, Winglee & Bohm 1997 where a steady asymptotic state is not obtained), etc. Furthermore, a gap

⋆E-mail: vlahakis@physics.uch.gr (NV); tsingan@physics.uch.gr (KT)

that the present model aspires to fill in the existing literature is the availability of a self-consistent MHD model for jet-type outflows wherein the jet speed is superfast at large distances from the base such that all perturbations are convected downstream to infinity and they do not destroy the steady-state solution.

In the following Section 2 the basic steps for a systematic construction of this class of models are outlined. In Section 3 we discuss the critical surfaces that select a physically interesting solution and in Section 4 the asymptotic behaviour of such solutions is briefly sketched. A detailed parametric study of the model, including the solution topologies, is given in Section 5 and finally in Section 6 the connection of the dimensionless parameters characterizing the present model to the observable physical quantities of collimated outflows is briefly sketched.

2 CONSTRUCTION OF THE MODEL

In this section we describe in some detail how our model can be systematically obtained from the closed set of the governing full MHD equations.

2.1 Governing equations

The *dynamics* of astrophysical outflows may be described to zeroth order by the well-known set of the steady ($\partial/\partial t = 0$) ideal hydromagnetic equations:

$$\rho(\boldsymbol{V}\cdot\nabla)\boldsymbol{V} = \frac{(\nabla\times\boldsymbol{B})\times\boldsymbol{B}}{4\pi} - \nabla P - \rho\nabla\mathcal{V} + \boldsymbol{F}_{\rm rad}\,, \tag{1}$$

$$\nabla\cdot\boldsymbol{B} = 0\,, \quad \nabla\cdot(\rho\boldsymbol{V}) = 0\,, \quad \nabla\times(\boldsymbol{V}\times\boldsymbol{B}) = 0\,, \tag{2}$$

where $\boldsymbol{B}$, $\boldsymbol{V}$, $-\nabla\mathcal{V} = -\nabla\left(-GM/r\right)$ denote the magnetic, velocity and external gravity fields, respectively, $\boldsymbol{F}_{\rm rad}$ the volumetric force of radiation, and ρ and P the gas density and pressure.

The *energetics* of the outflow on the other hand is governed by the first law of thermodynamics:

$$q = \rho\boldsymbol{V}\cdot\left[\nabla\left(\frac{1}{\Gamma-1}\frac{P}{\rho}\right) + P\nabla\frac{1}{\rho}\right], \tag{3}$$

where q is the volumetric rate of net energy input/output (Low & Tsinganos 1986), while $\Gamma = c_p/c_v$, with c_p and c_v the specific heats for an ideal gas.

With axisymmetry in spherical coordinates (r,θ,ϕ), the azimuthal angle ϕ is ignorable ($\partial/\partial\phi = 0$) and we may introduce the poloidal magnetic flux function $A(r,\theta)$, such that three free integrals of A exist. They are the total specific angular momentum carried by the flow and magnetic field, $L(A)$, the corotation angular velocity of each streamline at the base of the flow, $\Omega(A)$, and the ratio of the mass and magnetic fluxes, $\Psi_{\rm A}(A)$ (Tsinganos 1982). Then, the system of equations (1)–(2) reduces to a set of two partial and nonlinear differential equations, i.e., the r- and θ-components of the momentum equation on the poloidal plane. Note that by using the projection of the momentum equation along a stream-field line $A = $ const on the poloidal plane (r,θ), equation (3) becomes

$$\rho\boldsymbol{V}\cdot\nabla\left(\frac{1}{2}V^2 + \frac{\Gamma}{\Gamma-1}\frac{P}{\rho} + \mathcal{V} - \frac{\Omega r\sin\theta}{\Psi_{\rm A}}B_\phi\right) - \boldsymbol{V}\cdot\boldsymbol{F}_{\rm rad} = q\,. \tag{4}$$

For a given set of the integrals $L(A)$, $\Omega(A)$ and $\Psi(A)$, equations (1)–(3) can be solved to give $\rho(r,\theta)$, $P(r,\theta)$ and $A(r,\theta)$, *if* the heating function $q(r,\theta)$ and the radiation force $\boldsymbol{F}_{\rm rad}$ are known. Similarly, one may close this system of equations (1)–(3), *if* an extra functional relation of q with the unknowns ρ, P and A exists. As an example, consider the following *special* functional relation of q with these unknowns ρ, P and A (Tsinganos, Trussoni & Sauty 1992),

$$q = \frac{\gamma-\Gamma}{\Gamma-1}\frac{P}{\rho}\boldsymbol{V}\cdot\nabla\rho\,, \tag{5}$$

where $\gamma \le \Gamma$. Then, equation (3) can be integrated at once to give the familiar polytropic relation between P and ρ,

$$P = Q(A)\rho^\gamma\,, \tag{6}$$

for some function $Q(A)$ corresponding to the enthalpy along a poloidal surface $A = $ const. In this special case we can integrate the projection of the momentum equation along a stream-field line $A = $ const on the poloidal plane, equation (4), by further assuming that $\boldsymbol{V}\cdot\boldsymbol{F}_{\rm rad} = 0$, to get the well-known Bernoulli integral, which subsequently can be combined with the component of the momentum equation across the poloidal field lines (the transfield equation) to yield ρ and A. After finding a solution, one may go back to equation (3) and fully determine the function $q(r,\theta)$. It is evident that even in this *special* polytropic case with $\gamma \neq \Gamma$ the heating function q [not its functional form but the function $q(r,\theta)$ itself] can be found only a posteriori. Note that for $\gamma = \Gamma$ and only then the flow is isentropic.

Evidently, it is not possible to integrate equation (3) for *any* functional form of the heating function q, such as it was possible with the special form of the heating function given in equation (5). To proceed further then and find other more general solutions (effectively having a variable value for γ), one may choose some other functional form for the heating function q and from energy conservation, equation (3), derive a functional form for the pressure. Equivalently, one may choose a functional form for the pressure P and determine the volumetric rate of thermal energy a posteriori from equation (3), after finding the expressions of ρ, P and A that satisfy the two remaining components of the momentum equation. Hence, in such a treatment the heating sources that produce some specific solution are not known a priori; instead, they can be determined only a posteriori. However, it is worth keeping in mind that as explained before, this situation is analogous to the more familiar constant γ polytropic case, with $\gamma \neq \Gamma$. In this paper we shall follow this approach, which is further illustrated in the following section.

However, even by adopting this approach, the integration of the system of mixed elliptic/hyperbolic partial differential equations (1)–(2) remains a non-trivial undertaking. Besides their nonlinearity, the difficulty is largely owing to the fact that a physically interesting solution is constrained to cross some critical surfaces which are not known a priori but they are determined simultaneously with the solution. For this reason, only a very few such self-consistent solutions are available, albeit no one is superfast at infinity. Further assumptions on the shape of the critical surfaces are needed, as discussed in the following.

2.2 Assumptions

In order to construct analytically a new class of exact solutions, we shall proceed by making the following two key assumptions:

(i) that the Alfvén number M is solely a function of the dimensionless radial distance $R = r/r_\star$, i.e. $M = M(R)$
and

(ii) that the poloidal velocity and magnetic fields have a dipolar angular dependence,

$$A = \frac{r_\star^2 B_\star}{2}\mathcal{A}(\alpha)\,, \qquad \alpha = \frac{R^2}{G^2(R)}\sin^2\theta\,, \tag{7}$$

for some function $G(R)$.

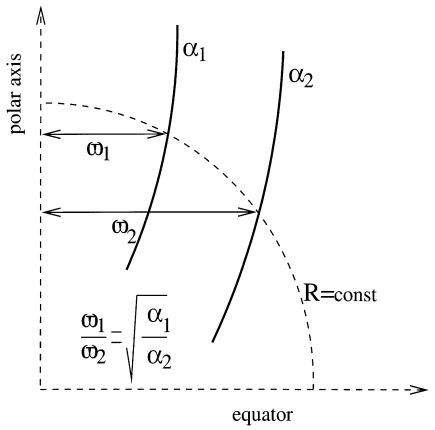

Figure 1. An illustration of the construction of the streamlines $\alpha = \text{const}$ on the poloidal plane in meridionally self-similar outflows.

A few words on the physical basis of the above two assumptions are needed at this point. We expect that assumptions (i)–(ii) are physically reasonable for describing the outflow properties at least close to the rotation and magnetic axis of the system. Far from the distortion caused by the presence of an accretion disc, the *angular* distribution of the stellar magnetic field may be approximately dipolar (cf. fig. 1 in Ghosh & Lamb 1979) in the vicinity of the polar axis. Also, regarding the assumption of spherical critical surfaces, we note that all available numerical models derive an approximately spherical shape for the Alfvén surface near the rotation and magnetic axis of the system (Sakurai 1985; Bogovalov & Tsinganos 1999; Ustyugova et al. 1999). Hence, although the analysed model may in principle extend to all polar angles as it satisfies the governing MHD equations, its physical applicability could be constrained around the polar regions only.

We are interested in trans-Alfvénic flows and denote by a subscript $\star$ the respective value of all quantities at the Alfvén surface. By choosing the function $G(R)$ such that $G(R=1)=1$ at the Alfvén transition $R=1$, it is evident that $G(R)$ measures the cylindrical distance ϖ to the polar axis of each field line labelled by α, normalized to its cylindrical distance ϖ_α at the Alfvén point, $G(R) = \varpi/\varpi_\alpha$. For a smooth crossing of the Alfvén sphere $R=1$ $[r = r_\star, \theta = \theta_{\rm a}(\alpha)]$, the free integrals L and Ω are related by

$$\frac{L}{\Omega} = \varpi_\alpha^2(A) = r_\star^2 \sin^2\theta_{\rm a}(\alpha) = r_\star^2 \alpha\,. \tag{8}$$

Therefore, the second assumption is equivalent to the statement that at the Alfvén surface the cylindrical distance ϖ_α of each magnetic flux surface $\alpha = \text{const}$ is simply proportional to $\sqrt{\alpha}$.

Instead of using the three remaining free functions of α, $(\mathcal{A}\,, \Psi_{\rm A}\,, \Omega)$, we found it more convenient to work instead with the three dimensionless functions of α, $(g_1\,, g_2\,, g_3)$,

$$g_1(\alpha) = \int \mathcal{A}'^2 {\rm d}\alpha\,, \tag{9}$$

$$g_2(\alpha) = \frac{r_\star^2}{B_\star^2}\int \Omega^2 \Psi_{\rm A}^2 {\rm d}\alpha\,, \tag{10}$$

$$g_3(\alpha) = \frac{\Psi_{\rm A}^2}{4\pi\rho_\star}\,. \tag{11}$$

These functions $g_1(\alpha)$, $g_2(\alpha)$, $g_3(\alpha)$ are vectors in a 3D α-space with some basis vectors $u_1(\alpha)$, $u_2(\alpha)$, $u_3(\alpha)$ (Vlahakis & Tsinganos 1998, hereafter VT98). Note that the forms of $g_1\,, g_2\,, g_3$ or equivalently the forms of A, Ψ_A, Ω, $L = r_\star^2\alpha\Omega$ and P should be such that the two remaining components of the momentum equation are separable in the coordinates α and R.

2.3 The method

The main steps of the general method for getting exact solutions under the previous two assumptions are given briefly in the following.

First, by using α instead of θ as the independent variable, we transform from the pair of independent variables $(R\,, \theta)$ to the pair of independent variables $(R\,, \alpha)$. The resulting form of the α-component of the momentum equation can be integrated at once to yield for the gas pressure

$$\begin{aligned} P(R,\alpha) &= \frac{B_\star^2}{8\pi}\left(f_0 + f_4 g_1 + f_1 g_1' + f_2 \alpha g_1' + f_5 g_2 + f_3 \alpha g_2'\right) \\ &= \frac{B_\star^2}{8\pi}\mathbf{Y}\mathbf{P}^\dagger\,, \end{aligned} \tag{12}$$

where $f_0(R)$ is a free function emerging from the integration, $f_i(R)$, $i = 1, 2, \ldots,$ are functions of the spherical radius R given in Appendix A, and $\mathbf{P}$ and $\mathbf{Y}$ are the (1×7) matrices

$$\mathbf{Y} = \left[\begin{array}{ccccccc} 1 & g_1 & g_1' & \alpha g_1' & g_2 & \alpha g_2' & g_3 \end{array}\right], \tag{13}$$

$$\mathbf{P} = \left[\begin{array}{ccccccc} f_0 & f_4 & f_1 & f_2 & f_5 & f_3 & 0 \end{array}\right]. \tag{14}$$

Secondly, by substituting equation (12) in the r-component of the momentum equation we obtain in terms of the (1×7) matrix $\mathbf{X}$,

$$\mathbf{X} = \left[\begin{array}{ccccccc} f_0' & f_4' & -f_6 & -f_7 & f_5' & -f_8 & -f_9 \end{array}\right], \tag{15}$$

the following equation:

$$\mathbf{Y}\mathbf{X}^\dagger = \mathbf{0}\,. \tag{16}$$

A key step in the method is to find a possible set of vectors $u_1(\alpha)$, $u_2(\alpha)$, $u_3(\alpha)$ such that all components of the matrix $\mathbf{Y}$ belong to the same α-space. To that goal we choose $u_1(\alpha) = 1$ and $u_2(\alpha) = g_1(\alpha)$. If this is the case, then our *third* step is to construct a 3×7 matrix $\mathbf{K}$ such that

$$\mathbf{Y} = \left[\begin{array}{ccc} u_1 & u_2 & u_3 \end{array}\right]\mathbf{K}\,. \tag{17}$$

Then, from equation (16),

$$\left[\begin{array}{ccc} u_1 & u_2 & u_3 \end{array}\right]\mathbf{K}\mathbf{X}^\dagger = \mathbf{0}\,,$$

and as u_i are linearly independent it follows that

$$\mathbf{K}\mathbf{X}^\dagger = \mathbf{0}\,. \tag{18}$$

Finally, it follows from equations (12), (14) and (17) that

$$P = \frac{B_\star^2}{8\pi}\left(P_0 + g_1 P_1 + u_3 P_2\right),$$

where the three components of the pressure P_0, P_1 and P_2 are

$$[P_0\ P_1\ P_2]^\dagger = \mathbf{K}\mathbf{P}^\dagger\,. \tag{19}$$

2.4 The model

Let us now apply this method to the construction of our specific model. We may recall that in a previous paper (VT98), it was found that only nine distinct general families of such vectors exist. One of them is

$$u_1(\alpha) = 1\,, \quad u_2(\alpha) = \alpha\,, \quad u_3(\alpha) = \alpha^\epsilon\,, \tag{20}$$

with the following free functions:

$$g_1(\alpha) = a\,, \tag{21}$$

$$g_2(\alpha) = \xi\alpha + \mu\alpha^{\epsilon}/\epsilon\,, \tag{22}$$

$$g_3(\alpha) = 1 + \delta\alpha + \mu\delta_0\alpha^{\epsilon}\,. \tag{23}$$

For this particular choice of $u_1(\alpha)$, $u_2(\alpha)$, $u_3(\alpha)$ we find the following form of the matrix $\mathbf{K}$,

$$\mathbf{K} = \begin{bmatrix} 1 & 0 & 1 & 0 & 0 & 0 & 1 \\ 0 & 1 & 0 & 1 & \xi & \xi & \delta \\ 0 & 0 & 0 & 0 & \dfrac{\mu}{\epsilon} & \mu & \mu\delta_0 \end{bmatrix}. \tag{24}$$

Then, from equations (14) and (19) we get

$$\begin{bmatrix} P_0 \\ P_1 \\ P_2 \end{bmatrix} = \begin{bmatrix} f_0 + f_1 \\ f_4 + f_2 + \xi\left(f_3 + f_5\right) \\ \mu\left(\dfrac{f_5}{\epsilon} + f_3\right) \end{bmatrix}. \tag{25}$$

Finally, from equation (18) and using the definitions of equations (15) and (24) we obtain the three *ordinary* differential equations, equations (B4), for the functions of R in the model for $\epsilon \neq 0, 1$ and $\mu \neq 0$ (only then do we have a 3D α-space with $1\,, \alpha\,, \alpha^{\epsilon}$ linearly independent).

Altogether, let us summarize the characteristics of our model. The physical quantities of the outflow have the following exact expressions:

$$\rho = \frac{\rho_\star}{M^2}\left(1 + \delta\alpha + \mu\delta_0\alpha^{\epsilon}\right), \tag{26}$$

$$P = \frac{\rho_\star V_\star^2}{2}\left(P_0 + P_1\alpha + P_2\alpha^{\epsilon}\right), \tag{27}$$

$$\boldsymbol{V} = V_\star\left(\frac{M^2\cos\theta}{G^2}\hat{r} - \frac{M^2 F\sin\theta}{2G^2}\hat{\theta} + .\sqrt{\xi\alpha + \mu\alpha^{\epsilon}}\,\frac{G^2 - M^2}{G\left(1 - M^2\right)}\hat{\phi}\right)\Big/\sqrt{1 + \delta\alpha + \mu\delta_0\alpha^{\epsilon}}\,, \tag{28}$$

$$\boldsymbol{B} = B_\star\left(\frac{\cos\theta}{G^2}\hat{r} - \frac{F\sin\theta}{2G^2}\hat{\theta} - \sqrt{\xi\alpha + \mu\alpha^{\epsilon}}\,\frac{1 - G^2}{G\left(1 - M^2\right)}\hat{\phi}\right), \tag{29}$$

where the five unknown functions $G^2(R)$, $F(R)$, $M^2(R)$, $P_1(R)$ and $P_0(R)$ entering in the above expressions are obtained from the integration of the five first-order ordinary differential equations given in Appendix B, while the pressure component $P_2(R)$ is given explicitly in terms of the other variables (Appendix B).

Note that the parameters ϵ and ξ determine the enclosed poloidal current by a given magnetic surface in the outflow. The parameters $\epsilon\,, \delta\,, \delta_0$ determine the latitudinal distribution of the density. The parameter μ controls the differential rotation. Further discussion of the physical meaning of these parameters will be given later (Sections 2.5, 5).

2.5 Some properties of the meridionally self-similar model

Our model is meridionally self-similar, i.e. if we know the shape of one field line $\alpha = \alpha_1$ we may derive the shape of any other streamline $\alpha = \alpha_2$ by moving in the meridional direction along each cycle $R = \text{const}$ on the poloidal plane as illustrated in Fig. 1.

Note that the flux function A is simply proportional to α which means that for cylindrical solutions at $R \gg 1$, the magnetic field on the poloidal plane is uniform and its strength is independent of α, $|\boldsymbol{B}_p|_\infty = B_\star/G_\infty^2$.

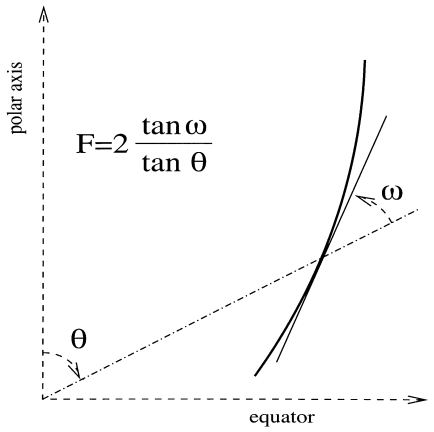

Figure 2. A geometrical illustration of the expansion factor $F(R)$, which determines the shape of the poloidal streamlines in a meridionally self-similar outflow. Usually, $1 < F < 2$ with $F = 1$ in conical and $F = 2$ in cylindrical expansion.

The density at the Alfvén surface is

$$\rho_\alpha = \frac{\Psi_A^2}{4\pi} = \rho_\star\left(1 + \delta\alpha + \mu\delta_0\alpha^{\epsilon}\right),$$

i.e. it is similar to a Taylor expansion in the cylindrical distance ϖ_α from the rotation and magnetic axis $\alpha = 0$. For example, for $\epsilon = 0.5$ we have

$$\frac{\rho_\alpha}{\rho_\star} = 1 + \mu\delta_0\frac{\varpi_\alpha}{r_\star} + \delta\left(\frac{\varpi_\alpha}{r_\star}\right)^2.$$

We have also introduced the expansion factor

$$F \equiv \frac{\partial \ln\alpha(R,\theta)}{\partial \ln R} = 2 - R\frac{G^{2'}}{G^2}\,,$$

which measures the opening of the field lines on the poloidal plane, as illustrated in Fig. 2. Thus, if $F > 2$ the field lines turn towards the axis, if $F = 2$ they expand cylindrically, if $F = 0$ they are purely radial, while if $F < 0$ the field lines turn toward the equator (in this case, there is a closed region near the equator). If we eliminate F in (B6) (using B5) we have the second derivative of G (which corresponds to the term $\partial^2 A/\partial r^2$ of the transfield equation). So, using F as an intermediate function we have only first-order differential equations.

2.6 Radiative acceleration

For the radiative acceleration we have assumed two components. The first component results from continuum absorption and is set proportional to the radiative flux. It decreases with distance as r^{-2}, similar to gravity. If L_ε is the Eddington luminosity, we may use the ratio $\Gamma_\varepsilon = L/L_\varepsilon$ such that this part of the radiative acceleration is $\Gamma_\varepsilon\rho\mathcal{G}M/r^2$.

We have also assumed a second component of the radiative acceleration resulting from line contribution. By adopting the optically thin atmosphere aproximation (Lamers 1986; Chen & Marlborough 1994; Kakouris & Moussas 1997), this part of the acceleration is simply a function of r as in general the total number of weak lines is a function of r. Then, the corresponding expression of the radiative acceleration is $\rho Q(R)V_\star^2/r_\star$.

The combination of gravitational and radiative acceleration is thus

$$-\rho\nabla\mathcal{V}+\boldsymbol{F}_{\rm rad}=\frac{V_\star^2}{r_\star}\rho\left(Q(R)-\frac{\nu^2}{2R^2}\right)\hat{r}\,,$$

where

$$\nu^2=\frac{V_{\rm esc}^2}{V_\star^2}\left(1-\Gamma_\varepsilon\right)=\frac{2GM}{r_\star V_\star^2}\left(1-\Gamma_\varepsilon\right).$$

Furthermore, we use for Q the approximation of a power law, $Q(R)=\mu_0/R^x$ with μ_0, and x constants.

In the following we shall discuss the results of the integration. Finally, we shall calculate all the other remaining physical quantities. A parametric study will be made only for $\epsilon>0$, because for $\epsilon<0$ we have $\rho\rightarrow\infty$ as $\alpha\rightarrow 0$.

For $\epsilon=0$ or 1 (or equivalently for $\mu=0$), we get a degenerate case that needs an extra condition between the functions of R. This case has been studied in Sauty & Tsinganos (1994) [where the components of the pressure $P_0\,,P_1$ are set proportional to each other] and Trussoni et al. (1997) [where the function $G(R)$ is given a priori]. Here, in the case $\mu=0$ we have chosen this extra condition to be $f_5/\epsilon-f_8-\delta_0 f_9=0$ (cf. the last equation of the system B4).

3 CRITICAL SURFACES

In the domain of the solutions, there exist several critical surfaces. In the following we briefly discuss the physical context of these critical surfaces.

3.1 Alfvén critical surface

We recall that one of our goals is to investigate transAlfvénic solutions wherein $L=\varpi_\alpha^2\Omega$. By multiplying equation (B6) with $1-M^2$ and evaluating the resulting expression at the Alfvén point we get

$$F_\star p_\star-\frac{F_\star^2-4}{2}-2P_{1\star}=0\,, \tag{30}$$

with $F_\star$, $P_{1\star}$ and $p_\star=\left({\rm d}M^2/{\rm d}R\right)_\star$ the respective values of these quantities at the Alfvén transition $R=1$. Equation (30) is the so-called Alfvén regularity condition in the present model. Note that if we also multiply (B8) with $1-M^2$ and evaluate the resulting expression at the Alfvén point we get an identical expression, while (B7) after using L'Hospital's rule gives an identity.

3.2 Slow/fast critical surfaces

In order to locate the critical surfaces where the radial component of the flow speed equals the corresponding slow/fast MHD wave speeds (Tsinganos et al. 1996), we need to calculate first the sound speed $C_{\rm s}$ at these points; to this goal we may proceed as follows.

Consider that at some fixed distance R of a given streamline labelled by α we make a small change in the density ρ and the pressure P. We may define the square of the sound speed as the ratio of such an infinitesimal change of P and ρ,

$$C_{\rm s}^2=\left(\frac{\partial P}{\partial\rho}\right)_{\alpha,R}=-\frac{V_\star^2}{2}\frac{M^4}{1+\delta\alpha+\mu\delta_0\alpha^\epsilon}\times\left[\frac{\partial P_0\left(R,M^2\right)}{\partial M^2}+\frac{\partial P_1\left(R,M^2\right)}{\partial M^2}\alpha+\frac{\partial P_2\left(R,M^2\right)}{\partial M^2}\alpha^\epsilon\right], \tag{31}$$

using (26)–(27). However, from the differential equation (B9) we can calculate the derivative $\partial P_0\left(R,M^2\right)/\partial M^2$, while from (B8) after substituting ${\rm d}F/{\rm d}R$ from equation (B6) we can calculate the other derivative $\partial P_1\left(R,M^2\right)/\partial M^2$. Finally, from equation (B10) by taking the derivative of $P_2(G,M^2)$ for constant $G(R)$ we similarly get the derivative $\partial P_2\left(R,M^2\right)/\partial M^2$. Substituting these derivatives in equation (31) we obtain the expression of the sound speed at the points where $\left(2M^2-1\right)G^4-M^4=0$.

An inspection of equation (B7) for the Alfvén number $M(R)$ reveals that besides the Alfvén transition where $M=G=R=1$, there may be other distances $R_x\neq 1$ where the denominator of this equation becomes zero, $\mathcal{D}\equiv\left[\left(2M^2-1\right)G^4-M^4\right]_{R=R_x}=0$. In such a case, the numerator of equation (B7) should be also set equal to zero and we have conditions typical of a critical point (using L'Hospital's rule we find two solutions for the slope of M^2 at this point, i.e., this singularity corresponds to an x-type critical point). To clarify the physical identity of such a critical point, we may manipulate the denominator $\mathcal{D}$ and write it in the form

$$\mathcal{D}=2\epsilon G^2\frac{1+\delta\alpha+\mu\delta_0\alpha^\epsilon}{V_\star^2V_{\rm A,r}^4\mu\alpha^\epsilon}\times\left(V_{\rm r}^2-V_{\rm A,r}^2\right)\left[V_{\rm r}^4-V_{\rm r}^2\left(C_{\rm s}^2+V_{\rm A}^2\right)+C_{\rm s}^2V_{\rm A,r}^2\right], \tag{32}$$

where $V_{\rm A}$, $V_{\rm A,r}$ are the total and radial Alfvén speeds, respectively. Evidently, a critical point at R_x corresponds to the fast/slow critical points modified by the meridional self-similarity (Tsinganos et al. 1996). In other words, the sphere $R=R_x$ is the corresponding spherical separatrix in the hyperbolic domain of the system of the MHD differential equations (Bogovalov 1996). The sound speed is well defined at the critical points where $\mathcal{D}=0$, but it is an open question whether this definition can be extended everywhere.

4 ASYMPTOTIC ANALYSIS

According to the asymptotical behaviour of the poloidal streamlines we may distinguish two different types of solutions.

4.1 Cylindrical asymptotics achieved through oscillations (Type I solutions)

In this case, the poloidal streamlines undergo oscillations of decaying amplitude and finally they become cylindrical. A similar oscillatory behaviour is found in all physical quantities, a situation that has already been analysed in detail (Vlahakis & Tsinganos 1997, henceforth VT97). According to this analysis, as $R\gg 1$ we have

$$M^2=M_\infty^2\left(1+\lambda_0\varepsilon\right),\quad G^2=G_\infty^2(1-\varepsilon)\,, \tag{33}$$

$$\varepsilon(r)\approx\frac{D}{r^s}\sin\left(kr+\phi_0\right),\quad s=2+\frac{\lambda_0M_\infty^2}{M_\infty^2-1}\,, \tag{34}$$

$$k^2=\frac{2\xi(1-\epsilon)\left(M_\infty^2-G_\infty^4\right)}{r_\star^2M_\infty^2\left(1-M_\infty^2\right)^2}\,, \tag{35}$$

$$\lambda_0=\left[(\epsilon+1)M_\infty^2-(\epsilon-1)G_\infty^4\right]\frac{1-M_\infty^2}{\left(2M_\infty^2-1\right)G_\infty^4-M_\infty^4}\,. \tag{36}$$

Note that for $s>1$ the gravitational term is dominant, but the analysis is still correct because the oscillatory perturbation is independent of the 'background' term $1/r$ (VT97).

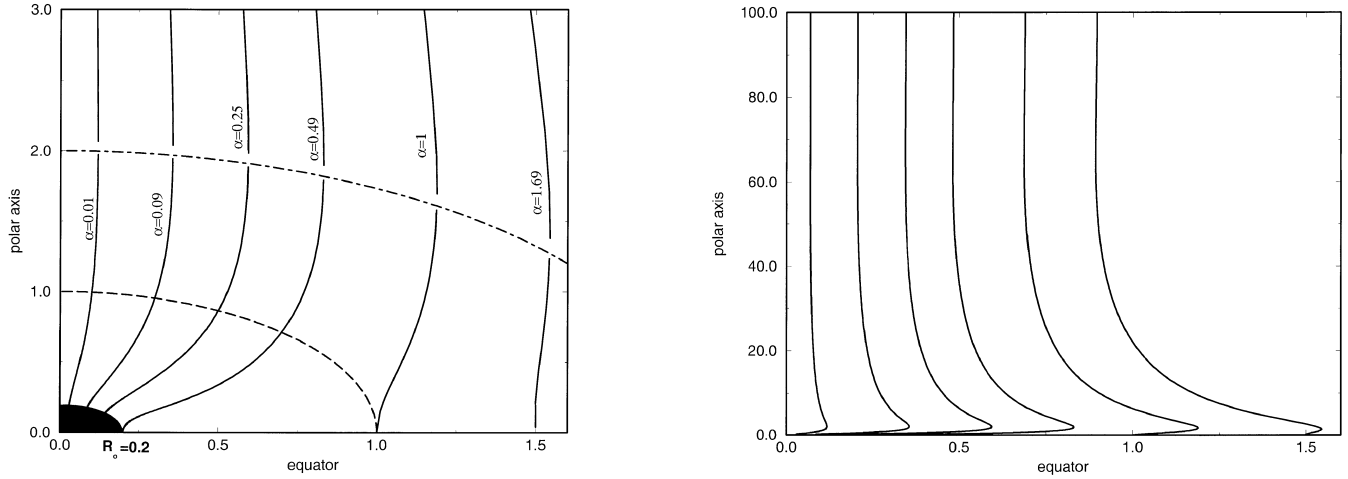

Figure 3. Poloidal streamlines near (left) and far (right) from the central object for case (a) with parameters: $\epsilon = 0.5$, $\xi = 10$, $\delta\nu^2 = 3.5$, $\delta_0\nu^2 = 0.1$, $\mu_0 = 0$, $F_\star = 1$ and $p_\star \approx 2.2655$. The Alfvén (fast) surface is indicated by dashed (dot–dashed) lines.

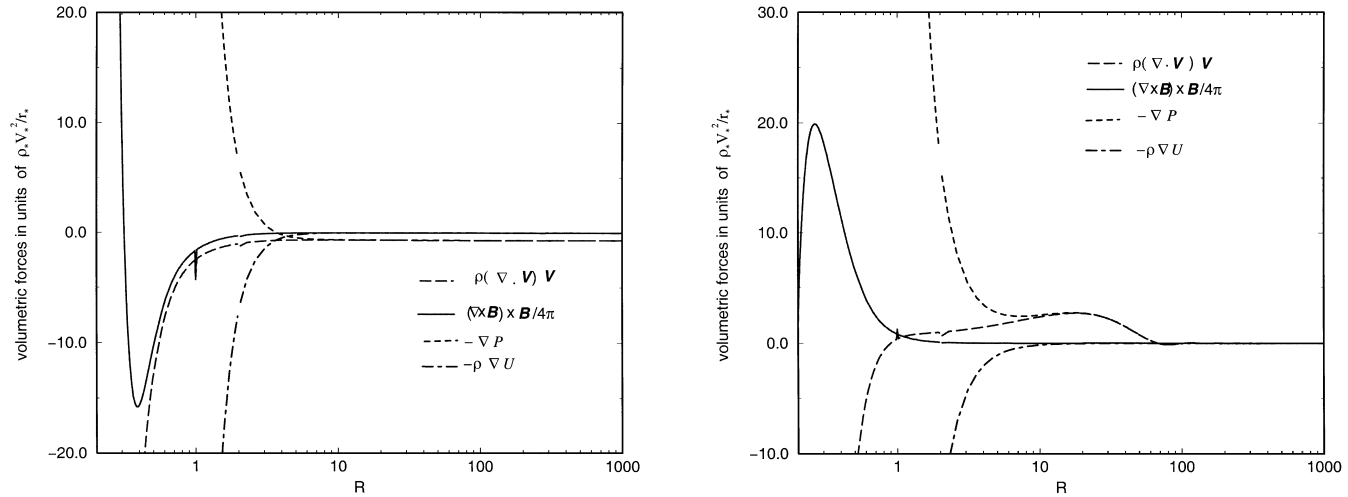

Figure 4. In the left panel are plotted the components of the magnetic (solid), pressure gradient (small dashes), gravitational (dot–dashed) and total acceleration (long dashes) perpendicular to the poloidal streamlines on line $\alpha = \alpha_{\rm lim}$ for the parameters of the previous figure. In the the right panel the corresponding components parallel to the poloidal lines are plotted also for case (a) and the same parameters: $\epsilon = 0.5$, $\xi = 10$, $\delta\nu^2 = 3.5$, $\delta_0\nu^2 = 0.1$, $\mu_0 = 0$, $F_\star = 1$ and $p_\star \approx 2.2655$.

4.2 Converging to the axis asymptotics (Type II solutions)

An analysis of the system of the differential equations (B6)–(B9) for $G(R \to \infty) \to 0$, $M(R \to \infty) \to \infty$ and $F(R \to \infty) \to F_\infty$ shows that in this case the value of the expansion factor F_∞ at $R \gg 1$ approaches a constant value, the positive root of the equation

$$(\epsilon + 3)\left(\epsilon + \frac{3}{2}\right)F_\infty^2 - 2(\epsilon + 2)\left(\epsilon + \frac{5}{2}\right)F_\infty - 4(\epsilon + 2) = 0\,.$$

As we shall see later, solutions are obtained mainly for $\epsilon > 0$, in which case this root is greater than 2, $F_\infty > 2$, i.e., the cross-sectional area of the flow tube drops to zero at large radii, $G^2 \propto R^{2-F_\infty}$. The poloidal velocity goes to infinity as $V_{\rm r} \propto R^{(\epsilon+2)(F_\infty-2)}$ to conserve mass, while the toroidal velocity grows like $V_\phi(R \to \infty) \propto R^{F_\infty-2}$ from angular-momentum conservation.

5 PARAMETRIC STUDY OF SOLUTIONS

The two crucial parameters that affect the qualitative behaviour of the model are ξ and ϵ. *First*, for ϵ, from the expression of the density ρ in equation (26), it is required that $\epsilon > 0$ in order that the density at the axis, $\rho(\alpha = 0, R)$ and the pressure are finite. In the case $\epsilon = 1$ the electric current $I_z(\alpha, R)$ enclosed by a poloidal magnetic flux tube $\alpha = {\rm const}$ and the corresponding confining azimuthal magnetic field $B_\phi(\alpha, R)$ are proportional to α; this case has already been studied by Sauty & Tsinganos (1994) and it was found that cylindrical asymptotes are obtained through oscillations. If $\epsilon > 1$, $I_z(\alpha, R)$ and $B_\phi(\alpha, R)$ increase faster with α, which results in a stronger magnetic pinching force, which eventually reduces the cross-sectional area of the flow tube to zero. Therefore, we expect that when $0 < \epsilon < 1$ we obtain asymptotic cylindrical solutions, while for larger values solutions where asymptotically $G_\infty \to 0$, as can be seen in Fig. 11. For the larger values of $\epsilon > 1$ the pinching is so strong that oscillations do not exist. This may also be seen from equation (35) where $k^2 < 0$ for $\epsilon > 1$ (for $\xi(M_\infty^2 - G_\infty^4) > 0$). Note that if $\epsilon > 1$, it is needed to have $\xi > 0$ such that the square roots in equations (B2), (B3) are positively defined near the axis $\alpha \approx 0$.

Overall then, we shall divide our parametric study accordingly into the intervals $0 < \epsilon < 1$, for cylindrical asymptotes with

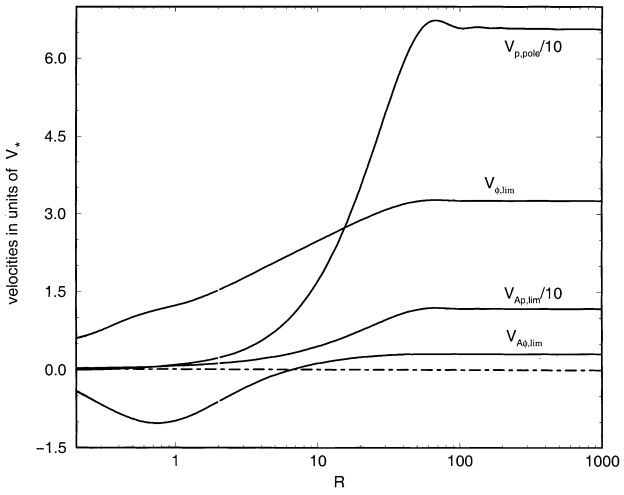

Figure 5. Dimensionless velocities for case (a) with parameters: $\epsilon = 0.5$, $\xi = 10$, $\delta\nu^2 = 3.5$, $\delta_0\nu^2 = 0.1$, $\mu_0 = 0$, $F_\star = 1$ and $p_\star \approx 2.2655$.

oscillations [cases (a)–(b)] and $\epsilon > 1$, for field lines converging to the axis without oscillations [case (c)].

Secondly, the parameter ξ is related to the asymptotic value of the pressure component P_1 (and through force balance in the cylindrical direction to B_ϕ and I_z). For cylindrical solutions at $R \gg 1$, we get from the asymptotic analysis

$$P_{1,\infty} = -\xi\left[\frac{(M^2-1)(G^4-M^2)+M^2(1-G^2)^2}{G^2M^2(1-M^2)^2}\right]_\infty .$$

For example when $\xi > 0$, in which case from the integration we find $G_\infty < 1 \ll M_\infty$, we obtain $P_{1,\infty} > 0$ and the pressure gradient assists the magnetic pressure in collimating the outflow. In that respect solutions with $\xi > 0$ correspond to an underpressured jet (Trussoni et al. 1997). On the other hand when $\xi < 0$, in which case from the integration $G_\infty^4 > M_\infty^2 > 1$, we find $P_{1,\infty} > 0$, $P_{2,\infty} < 0$. In all solutions with cylindrical asymptotes (i.e. for $\epsilon < 1$), one finds that for $\xi > 0$ the total pressure force in the $\hat{\boldsymbol{\varpi}}$ direction $-\hat{\boldsymbol{\varpi}}\nabla\left[P + B^2/(8\pi)\right]$ is towards the axis while for $\xi < 0$ it is in the opposite direction.

In all these cases we have $\xi(M_\infty^2 - G_\infty^4) > 0$, or $\xi\left[\left(\rho V_{\rm r}^2/2\right)_{\alpha=0,R\gg1} - \left(\rho V_{\rm r}^2/2\right)_{\alpha=0,R=1}\right] > 0$. In other words the sign of ξ determines if the poloidal kinetic energy on the axis is larger at the Alfvén point or at infinity. Thus, according to the range of values of ξ and ϵ we distinguish the following cases.

5.1 Case (a): $0 < \epsilon < 1$, $\xi > 0$

In this case cylindrical asymptotes are achieved through small-amplitude oscillations of decaying amplitude (Type I solutions). In

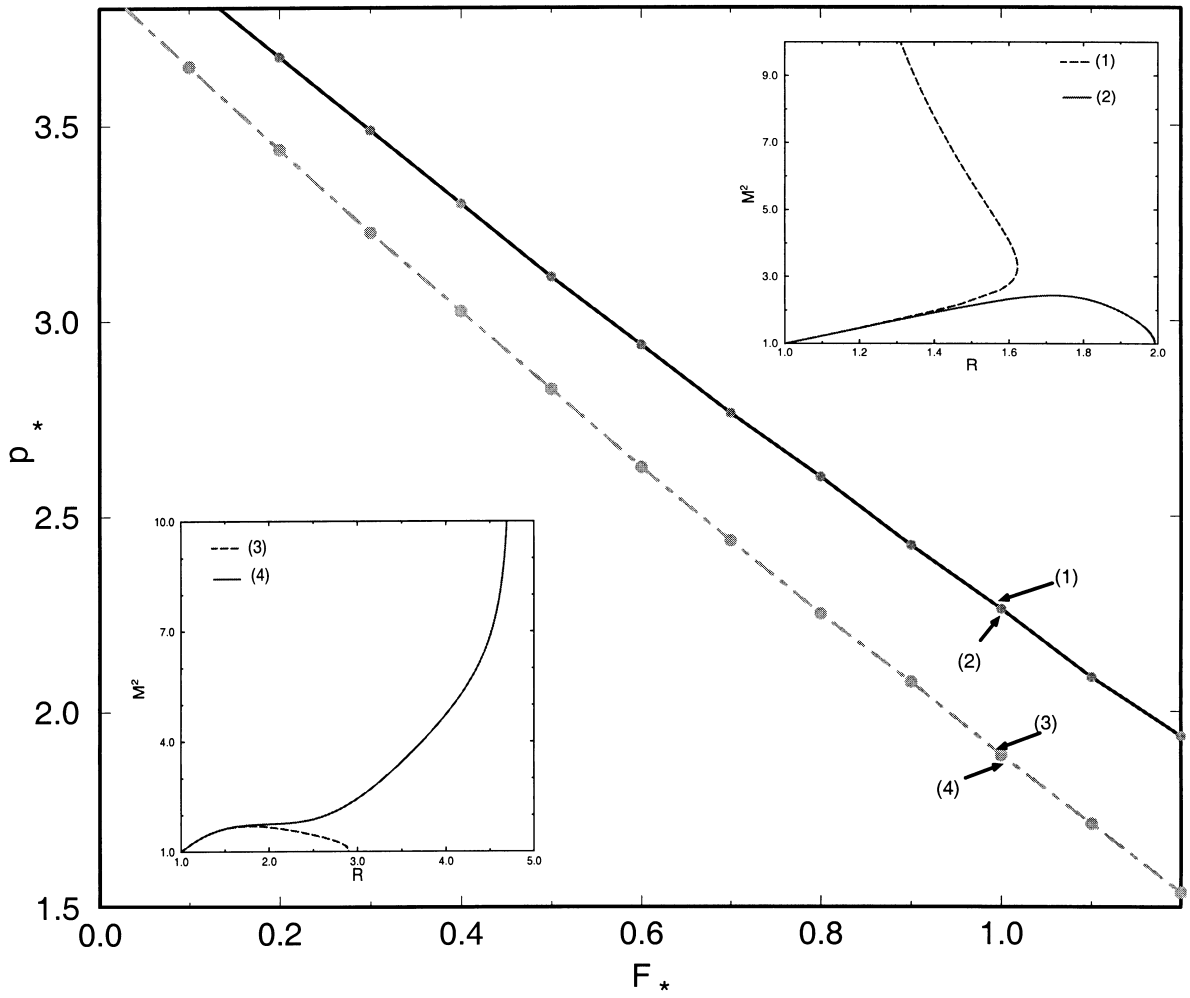

Figure 6. The solid line gives the relation between the expansion factor $F_\star$ and the slope $p_\star$ of $M^2(R)$ at the Alfvén point for a solution through all critical points, for case (a) with parameters: $\epsilon = 0.5$, $\xi = 10$, $\delta\nu^2 = 3.5$, $\delta_0\nu^2 = 0.1$, $\mu_0 = 0$. The topologies of $M^2(R)$ at the neighbouring points (1), (2), (3) and (4) are also shown.

the left panel of Fig. 3 the shape of the field/streamlines on the poloidal plane is shown in the inner region between the stellar base, the Alfvén (dashed, $R = 1$) and fast (dot–dashed, $R = 2$) critical surfaces. The poloidal lines are almost radial up to the Alfvén surface while after the fast critical surface they have attained a cylindrical shape. However, the final cylindrical shape of the poloidal field/streamlines is reached further out, i.e. at about $R = 20$, as it is shown in the larger scale of Fig. 3 (right panel), where their asymptotically cylindrical shape can be better seen. The bending of the poloidal field/streamlines towards the magnetic/rotational axis is caused by the magnetic pinching force as it can be seen in the left panel of Fig. 4 where the various components of the forces acting on the plasma perpendicular to the poloidal field lines are plotted. In the inner region of the outflow, the total inertial force perpendicular to the lines (centripetal force) is almost exclusively provided by the inwards magnetic force, with the outwards pressure gradient balancing the inward component of gravity. Asymptotically however, the magnetic pinching force and gravity are negligible and the pressure gradient of the underpressured jet balances the centrifugal force. The acceleration of the plasma along the poloidal lines can be seen in the right panel of Fig. 4. Evidently, in the inner region gravity is balanced by the pressure gradient force and the plasma is accelerated only by the remaining magnetic force while in the outer region where gravity and the magnetic force are negligible, it is accelerated by the dominant pressure gradient force. As it may also be seen in Fig. 5 most of the acceleration occurs on the far region at $R \gtrsim 10$ by the thermal pressure gradient force.

The solution discussed in this representative example crosses the fast critical point modified by self-similarity and a note is in order here to explain how such a solution may be obtained. First, we integrate equations (B6)–(B9) downstream of the Alfvén critical point at which $R = G = M = 1, F = F_\star, P_1 = P_{1\star}$ and $P_0 = P_{0\star}$, a free parameter that determines the pressure at infinity. At $R = 1$, the Alfvén regularity condition relates $F_\star$, $p_\star$ and $P_{1\star}$, equation (30). Also there is a relation between $F_\star$,$p_\star$ such that the solution passes through the fast critical point; this is the solid line in Fig. 6. Assume for example that we choose $F_\star = 1$ and we vary $p_\star$, Fig. 6. There is only one value of $p_\star \approx 2.26$ that satisfies the Alfvén regularity condition and the solution crosses the fast critical point. For other values of $p_\star$ above and below $p_\star \approx 2.26$ we have three different types of unphysical solutions shown in Fig. 6:

(i) from point (1) of Fig. 6 corresponding to $p_\star$ higher than 2.26 we get solutions in which the denominator of the differential equation for M^2 becomes zero and the curve $M^2(R)$ turns back to smaller distances;

(ii) from point (2) of Fig. 6 corresponding to $p_\star$ lower than 2.26 until point (3) we get solutions in which the numerator of the differential equation for M^2 becomes zero and then the solutions become again subAlfvénic;

(iii) finally, from point (4) of Fig. 6 we get solutions in which there is a distance R wherein $M \to \infty$ and the solutions terminate there.

A fine tuning between points (1) and (2) gives the unique solution that goes to infinity with superAlfvénic and superfast radial velocity, satisfying also the causality principle for the propagation of MHD perturbations. After finding such a critical value for $p_\star$ we also integrate equations (B6)–(B9) upstream of the Alfvén point.

5.2 Case (b): $0 < \epsilon < 1$, $\xi < 0$

In this case we may have two possibilities. In one, the solution crosses the fast critical point and the situation is similar to the previous case (a). However, at the same time asymptotically cylindrical solutions exist which do not cross the modified fast critical point, being simply superAlfvénic. An example of this type of behaviour is shown in Figs 7–10. As in case (a), cylindrical asymptotes are achieved through oscillations of decaying amplitude (Type I solutions). In the left panel of Fig. 7 the shape of the field/streamlines on the poloidal plane is shown in the inner region between the stellar base and the Alfvén (dashed, $R = 1$) critical surface. The poloidal lines are almost radial up to this Alfvén surface while outside $R = 1$ they attain a cylindrical shape. However, the final cylindrical shape of the poloidal field/streamlines is reached further out, i.e. at about $R = 20$, as it is shown in the larger scale of the right panel of Fig. 7 where their asymptotically cylindrical shape obtained through the decaying amplitude oscillations can be better seen.

As in case (a), the focusing of the poloidal field/streamlines towards the magnetic and rotation axis is caused predominantly by the magnetic pinching force; this may be seen in the left panel of Fig. 8 where the various components of the forces acting on the plasma *perpendicular* to the poloidal field lines are plotted. In the inner region of the outflow $R \lesssim 1$, the total inertial force perpendicular to the lines (centripetal force) is almost exclusively provided by the inwards magnetic force. In the far zone where gravity is negligible, $R \gtrsim 1$, the inwards magnetic pinching force is balanced by the pressure gradient of the overpressured jet and the centrifugal force. The acceleration of the plasma *along* the poloidal lines can be seen in the right panel of Fig. 8. In the inner region $R \lesssim 1$ the magnetic and pressure gradient forces accelerate the plasma; in the outer region where gravity and the magnetic forces are negligible, the pressure gradient force is left alone to accelerate the plasma. As in case (a), it may also be seen in the right panel of Fig. 8 that most of the acceleration occurs in the far region at $R \approx 10$ caused by the thermal pressure gradient force.

Fig. 9 is a plot of the values of $p_\star$ and $F_\star$ for which the fast point is crossed. As in case (a), we integrate equations (B6)–(B9) downstream of the Alfvén critical point at which $R = G = M = 1$, $F = F_\star$, $P_1 = P_{1\star}$ and $P_0 = P_{0\star}$. At $R = 1$ the Alfvén regularity condition relates $F_\star$, $p_\star$ and $P_{1\star}$, equation (30). Also there is a relation between $F_\star$,$p_\star$ such that the solution passes through the fast critical point; this is the solid line in Fig. 9. Assume for example that we choose $F_\star = 0.7$ and we vary $p_\star$ (Fig. 9). There is only one value of $p_\star \approx 2.6$ that satisfies the Alfvén regularity condition and the solution crosses the fast critical point. For other values of $p_\star$ above and below $p_\star \approx 2.6$ we have different types of solutions shown in Fig. 9:

(i) at point (6) of Fig. 9 corresponding to $p_\star$ higher than $p_\star \approx 2.6$ we get solutions in which the denominator of the differential equation for M^2 becomes zero and the curve $M^2(R)$ turns back to smaller distances;

(ii) at points (5), (4) and (1) of Fig. 9 we get solutions in which the numerator of the differential equation for M^2 becomes zero and then the solutions become again subAlfvénic;

(iii) at points (2) and (3) of Fig. 9 we get oscillatory solutions that do not cross the fast critical point. These solutions are shown in Figs 7 and 8.

A fine tuning between points (6) and (5) gives the unique solution that goes to infinity with superAlfvénic and superfast radial velocity.

Note that in this case there exists a value $\alpha_{\rm out}$ where $V_\phi = 0$ and $B_\phi = 0$. In this streamline the enclosed poloidal current is zero. For $\mu = 9$ and the parameters as in Fig. 7, $\alpha_{\rm out} = 3.24$.

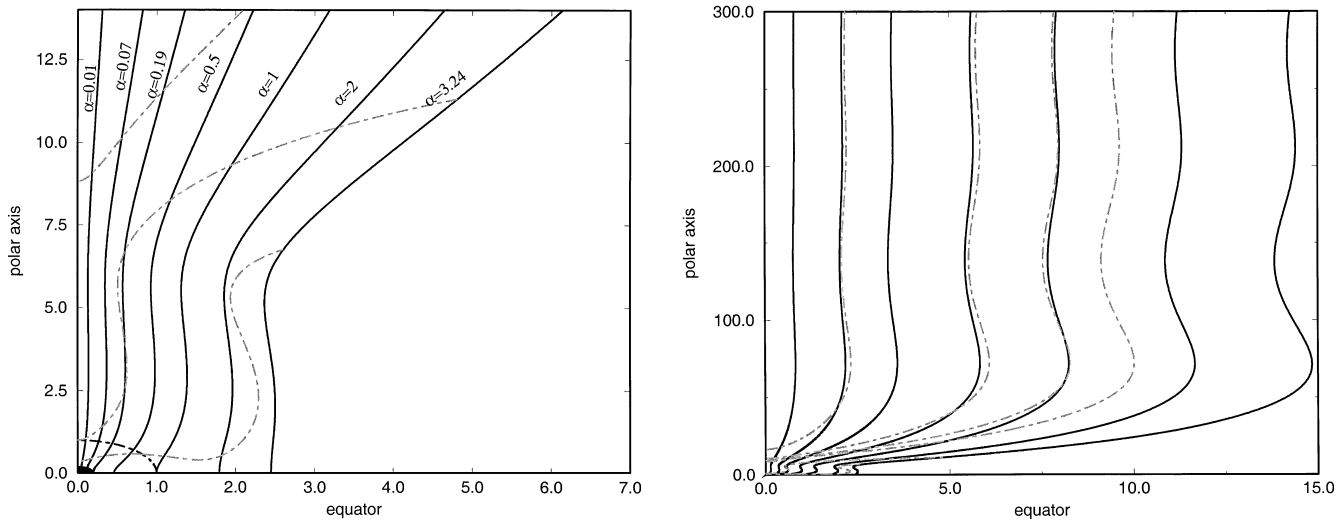

Figure 7. Poloidal streamlines near (left) and far (right) from the central object for case (b) with parameters: $\epsilon = 0.5$, $\xi = -5$, $\delta\nu^2 = 4$, $\delta_0\nu^2 = 0.001$, $\mu_0 = 0$, $F_\star = 1$ and $p_\star = 2$. With dotted lines the density isocontours are indicated with $\rho/\rho_\star = 0.1, 1, 10$ from top to bottom in the left panel and $\rho/\rho_\star = 0.01, 0.04, 0.07, 1, 10$ from left to right in the right panel. The Alfvén surface in the left panel is indicated by dashed lines.

5.3 Case (c): $\epsilon > 1$, $\xi > 0$

As discussed in the beginning of Section 5, when $\epsilon > 1$ the strong magnetic pinching force results in a jet of zero asymptotic radius; in addition, this asymptote is achieved without oscillations, i.e., we obtain Type II solutions (Figs 11–13). The values of $p_\star$ and $F_\star$ for which the solution crosses the fast critical point are shown in Fig. 12.

As with the previous cases, for each value of $F_\star$ there is only one value of the Alfvén number slope $p_\star$ for which the solution passes through the fast critical point; this is the solid line in Fig. 12. Assume for example that we choose $F_\star = 0.8$ and we vary $p_\star$ (Fig. 12). There is only one value of $p_\star \approx 2.53$ that satisfies the Alfvén regularity condition and the solution crosses the fast critical point. For other values of $p_\star$ above and below $p_\star \approx 2.53$ we have two different types of unphysical solutions shown in Fig. 12:

(i) at point (1) of Fig. 12 corresponding to $p_\star$ higher than 2.53 we get solutions in which the denominator of the differential equation for M^2 becomes zero and the curve $M^2(R)$ turns back to smaller distances;

(ii) at point (2) of Fig. 12 corresponding to $p_\star$ lower than 2.53 we get solutions in which the numerator of the differential equation for M^2 becomes zero and then the solutions again become subAlfvénic.

Fine tuning between points (1) and (2) gives the unique solution that goes to infinity with superAlfvénic and superfast radial velocity. Nevertheless, the jet radius goes to zero in this case.

6 ASTROPHYSICAL APPLICATIONS

It should be noted that the purpose of this paper has not been to construct a specific model for a given collimated outflow; instead, our goal has been to outline via a specific class of exact

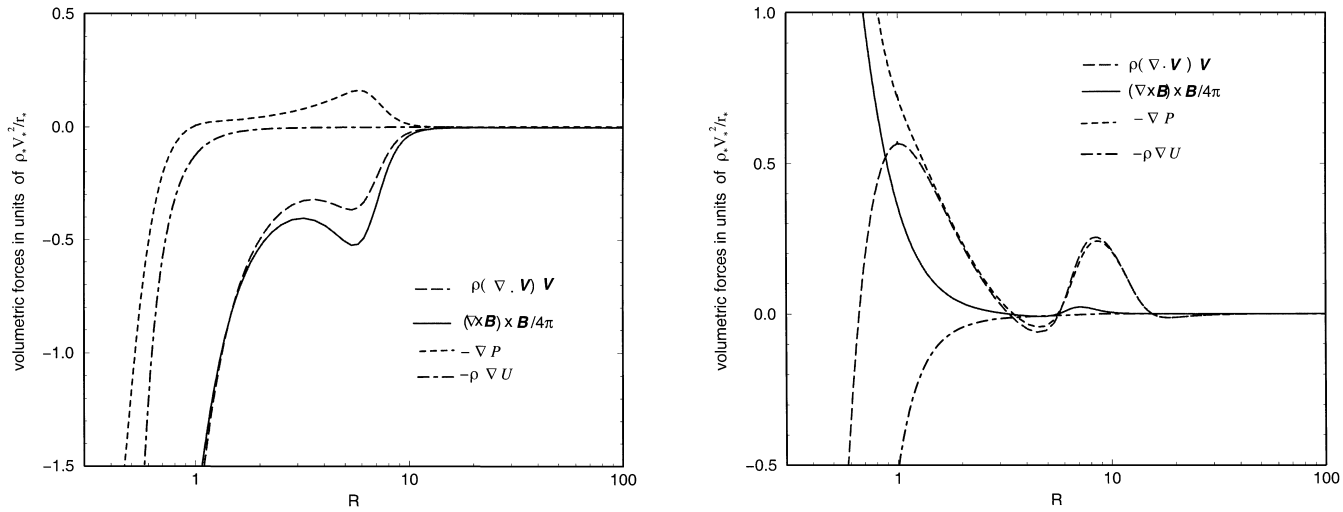

Figure 8. In the left panel are plotted the components of the magnetic (solid), pressure gradient (small dashes), gravitational (dot–dashed) and total acceleration (long dashes) perpendicular to the poloidal streamlines on line $\alpha = \alpha_{\rm lim}$. In the right panel the corresponding components parallel to the poloidal lines are plotted also for case (b) and the same set of parameters: $\epsilon = 0.5$, $\xi = -5$, $\delta\nu^2 = 4$, $\delta_0\nu^2 = 0.001$, $\mu_0 = 0$, $F_\star = 1$ and $p_\star = 2$.

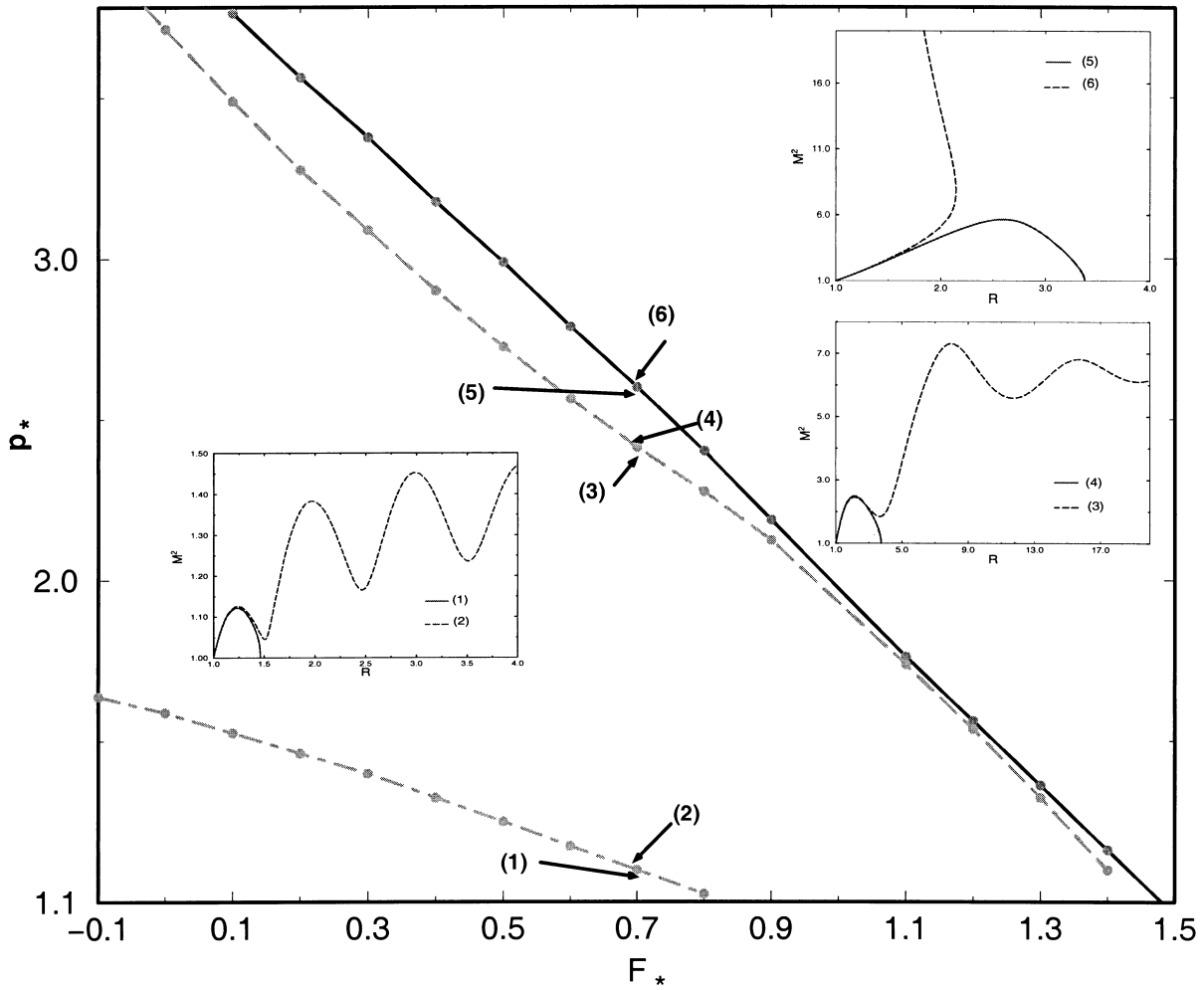

Figure 9. The solid line gives the relation between the expansion factor $F_\star$ and the slope $p_\star$ of $M^2(R)$ at the Alfvén point for a solution through all critical points, for case (b) with parameters: $\epsilon = 0.5$, $\xi = -5$, $\delta\nu^2 = 4$, $\delta_0\nu^2 = 0.001$, $\mu_0 = 0$. The topologies of $M^2(R)$ at the neighbouring points (1) to (6) are also shown.

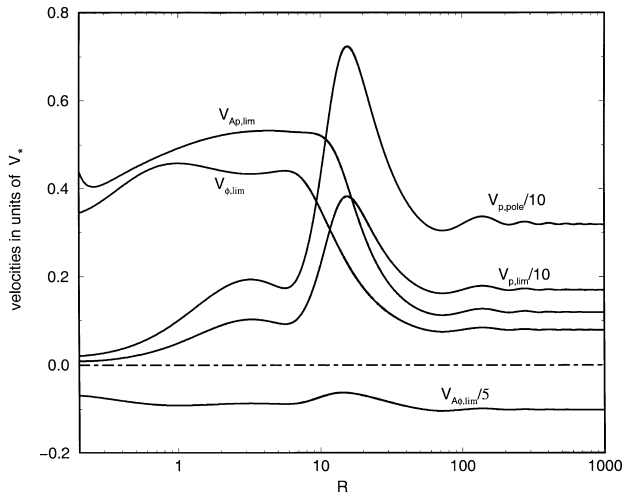

Figure 10. Dimensionless velocities for case (b) with parameters: $\epsilon = 0.5$, $\xi = -5$, $\delta\nu^2 = 4$, $\delta_0\nu^2 = 0.001$, $\mu_0 = 0$, $F_\star = 1$ and $p_\star = 2$.

and self-consistent models, the interplay of the various MHD processes contributing into the acceleration and collimation of jets. Nevertheless, the illustrative examples analysed in this paper can be compared with the observable characteristics of outflows from stellar or galactic objects, say, those associated with young stellar objects. For this purpose, in the following we establish the connection between the non-dimensional models and the observable parameters of the outflow.

Suppose that at the polar direction of the stellar surface ($r = r_0\,, \alpha = 0$) we know the values of $V_{\rm r}\,, B_{\rm r}$ and ρ, say, V_0, B_0 and ρ_0, respectively, such that we calculate $M_0 = V_0\sqrt{4\pi\rho_0}/B_0$. From the integration we can find the distance R_0 where $M(R_0) = M_0$. Thus, we may calculate the Alfvén distance $r_\star = r_0/R_0$. Each line that has its footpoint on the stellar surface at angle θ_i is labelled by $\alpha = \left[r_0 \sin\theta_i / r_\star G\left(r_0/r_\star\right)\right]^2$. The last line originating from the star is $\alpha_{\rm lim}$. Each line that has its footpoint on the disc at distance $r_i > r_0$ from the axis of rotation is labelled by $\alpha = \left[r_i/r_\star G\left(r_i/r_\star\right)\right]^2 > \alpha_{\rm lim}$.

If at the stellar surface $G(R_0) = G_0$ we find the Alfvén values, $V_\star = V_0 G_0^2/M_0^2$, $B_\star = B_0 G_0^2$, $\rho_\star = \rho_0 M_0^2$ and from equations (26)–(29) we can find all physical quantities at any point. For example at $R \gg 1$, $\alpha = 0$ we have the following asymptotic values: $V_\infty = V_0 G_0^2 M_\infty^2/M_0^2 G_\infty^2$, $B_\infty = B_0 G_0^2/G_\infty^2$, $\rho_\infty = \rho_0 M_0^2/M_\infty^2$.

6.1 Model of case (a)

For a typical solution with parameters as those plotted in Fig. 3, the values of characteristic physical quantities are shown in Table 1.

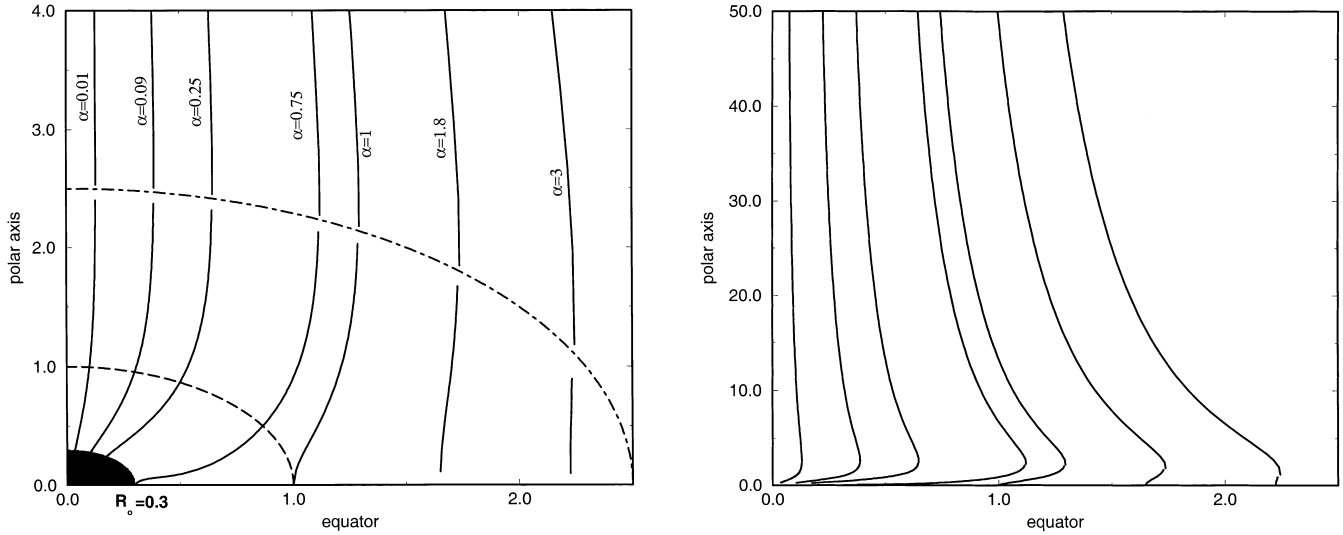

Figure 11. Poloidal streamlines near (left) and far (right) from the central object for case (c) with parameters: $\epsilon = 2$, $\xi = 10$, $\delta\nu^2 = 4$, $\delta_0\nu^2 = 0.1$, $\mu_0 = 0$, $F_\star = 0.8$ and $p_\star \approx 2.5636$. The Alfvén (fast) surface is indicated by dashed (dot–dashed) lines.

These values refer to the intersection of the rotational axis with (i) the stellar surface, (ii) the Alfvén singular surface, (iii) the fast singular surface modified by the self-similarity and (iv) infinite distance from the source. For a solar-type stellar mass 2×10^{33} g we have $\nu^2 = 462$, while for $\mu = 0.01$ the angular velocity at the equatorial point of the stellar surface has the solar value $2 \times 10^{-6}\,\mathrm{s}^{-1}$. Note that in this case (a) the toroidal component of the magnetic field changes sign at some spherical surface (cf. the velocity $V_{\mathrm{A}\phi,\mathrm{lim}}$ in Fig. 5. This means that the poloidal current enclosed by this surface is zero. All field lines that pass through this surface have the same cylindrical distance from the axis with the Alfvén point ($G = 1$ at this spherical surface) while for larger distances $G < 1$. After crossing this surface the Poynting flux changes its sign and thus the toroidal component of the velocity becomes large enough [because $V_\phi/\varpi\Omega = \left(M^2 - G^2\right)/G^2\left(M^2 - 1\right) \approx 1/G^2$]. It is worth noting that even with such rather weak strengths of the magnetic field, collimation is readily achieved.

6.2 Model of case (b)

For a typical solution with parameters such as those plotted in Fig. 7, the values of characteristic physical quantities are also shown in Table 1 and these values refer, as before, to the intersection of the rotational axis with (i) the stellar surface, (ii) the Alfvén singular surface and (iv) infinite distance from the source. The last line connected with the star has $\alpha_{\mathrm{lim}} = 0.19$ while the disc has a radius 2.45×10^{12} cm. If we choose a one solar mass star, $\nu^2 = 0.3$ while for $\mu = 9$, the stellar equator rotates with a speed $2.7 \times 10^4\,\mathrm{cm\,s}^{-1}$ (the angular velocity is $1.3 \times 10^{-7}\,\mathrm{s}^{-1}$).

The asymptotic radius of the jet (which is bounded with the line α_{out}) is 1 au, while the part of the flow starting from the stellar surface has a radius 0.23 au.This part of the jet is collimated at a distance of about 4 au from the equatorial plane, while the whole solution collimates at a height of 3.3 au. These results are consistent with recent observations of YSOs (Ray et al. 1996).

6.3 Model of case (b) including radiation

There are two parameters (μ_0 , x) determining the radiative force (the third is included in ν^2). For the parameters of case (b) but for $\mu_0 \neq 0$, we examine the effect of the radiative force on the velocity and the asymptotic radius of the outflow. As we expect, as the radiative force increases, the terminal velocity becomes larger, Fig. 14, while the Alfvén surface moves closer to the stellar base. From mass conservation we expect that the cross-sectional area of the jet decreases as x increases, as it is shown in Fig. 15.

7 SUMMARY AND CONCLUSIONS

In this paper we have examined a class of exact solutions of the set of the MHD equations (1)–(2) governing the dynamics of a magnetized outflow from a rotating gravitating object. For this system to be closed, an additional equation is needed to describe the energetics of the outflow, i.e. some form of the energy conservation principle, equation (3). The often used simplifying polytropic relationship between pressure and density that corresponds to a specific functional form of the net heating/cooling in the plasma was not used. This has the inconvenient consequence that the sound speed is ill-defined and it can be calculated only at the critical points. Besides this inconvenience we do not suffer any loss of generality in adopting a more general functional form of the total heating than the polytropic assumption implies. As explained in Section 2, in both the familiar polytropic case of constant γ and the present non-constant γ approach, the detailed spatial distribution of the required heating can be calculated only a posteriori.

The class of solutions that is analysed in this paper belongs to a group of nine classes of meridionally self-similar MHD solutions, which have been shown to exist in the recent paper VT98 under the assumptions that the Alfvén–Mach number is a function of the radial distance and the poloidal magnetic field has a dipolar angular dependence (equation 7). These assumptions may be reasonable for outflows around the magnetic and symmetry axis of the system. No assumption was made about the asymptotes of the outflows. It is interesting that the self-consistently deduced shape of the streamlines and magnetic field lines was found to be helices wrapped around surfaces that are asymptotically cylindrical. In other words, the streamlines extended to infinite heights above the central object and its disc obtaining the form of a jet. It was shown that such collimation is obtained even with very weak magnitudes of the

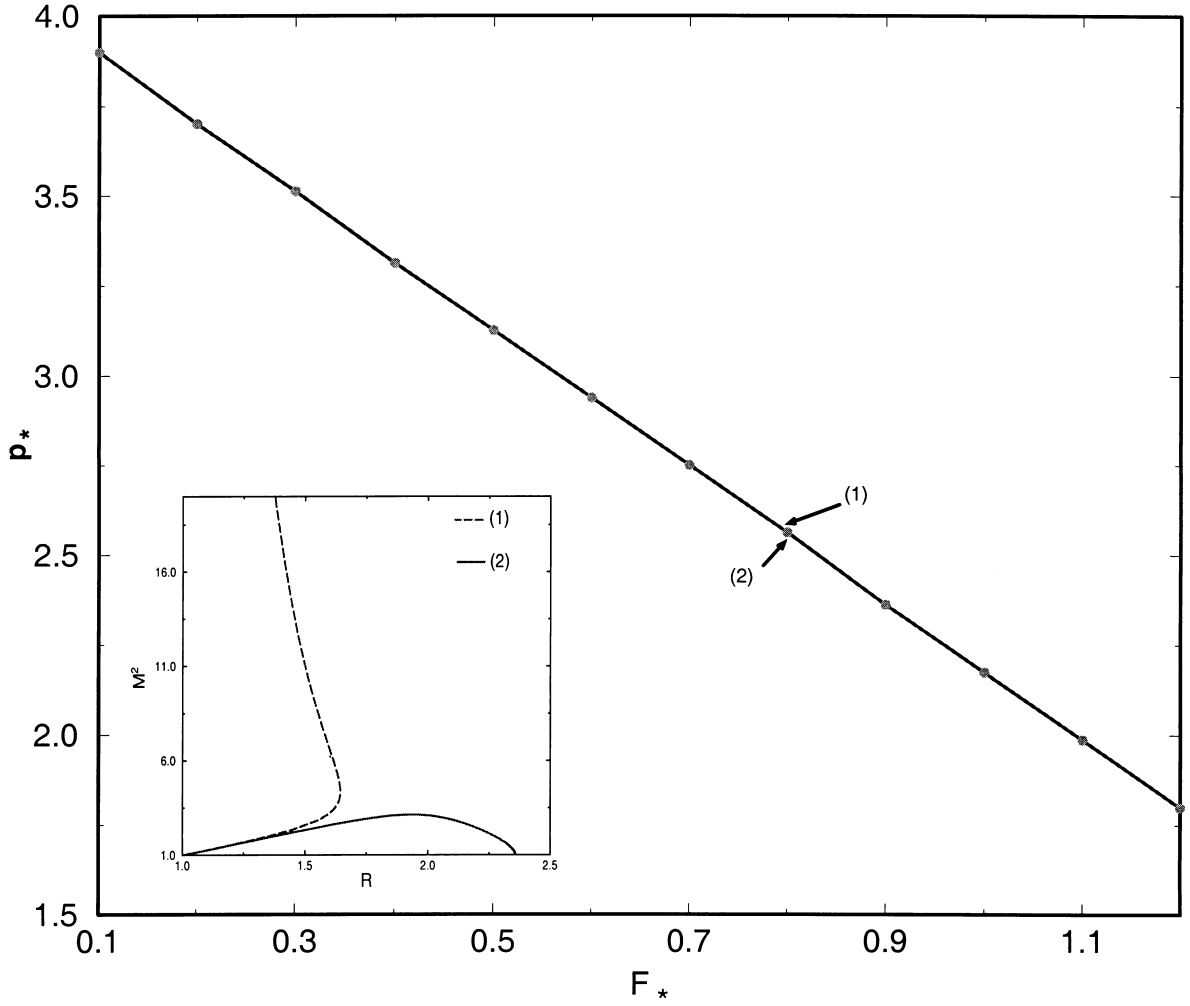

Figure 12. The solid line gives the relation between the expansion factor $F_\star$ and the slope $p_\star$ of $M^2(R)$ at the Alfvén point for a solution through all critical points, for case (c) with parameters: $\epsilon = 2$, $\xi = 10$, $\delta\nu^2 = 4$, $\delta_0\nu^2 = 0.1$, $\mu_0 = 0$.

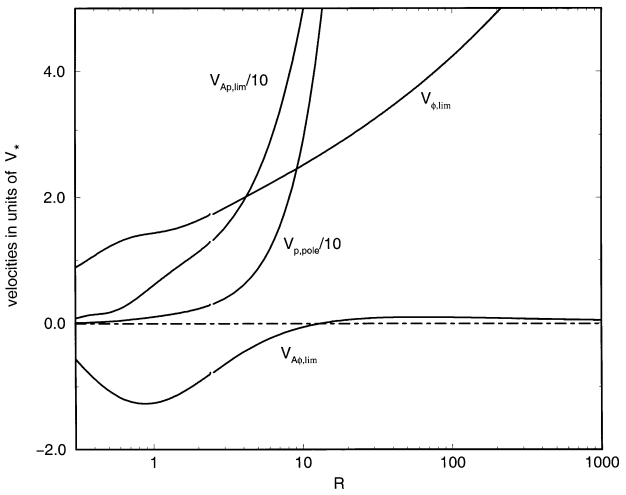

Figure 13. Dimensionless velocities for case (c) with parameters: $\epsilon = 2$, $\xi = 10$, $\delta\nu^2 = 4$, $\delta_0\nu^2 = 0.1$, $\mu_0 = 0$, $F_\star = 0.8$ and $p_\star \approx 2.5636$.

magnetic field. This result may be contrasted to the quite frequently referred to Blandford & Payne (1982) solutions, which by overfocusing towards the axis terminate at finite heights above the disc. The new element that the present model introduces in the self-consistent modelling of MHD outflows is that it produces for the first time jet-type solutions extending from the stellar base to infinity and where the outflow crosses at a finite distance the fast critical point such that the MHD causality principle is satisfied. The cylindrical asymptotes of the present non-polytropic solutions are consistent with the polytropic analysis of Heyvaerts & Norman (1989) and also with the class of superAlfvénic but subfast solutions at infinity of Sauty & Tsinganos (1994) for efficient magnetic rotators. However, no radial asymptotes were found in the present class of models, contrary to the other class of meridionally self-similar solutions examined in Sauty & Tsinganos (1994) where for inefficient magnetic rotators radial asymptotes have been found; it may be that the present model belongs to the group of efficient magnetic rotators.

The topologies of the solutions are rather rich as it was shown in the plane defined by the slope of the Alfvén number $p_\star$ and the streamline expansion factor $F_\star$ at the Alfvén transition. For example, for a given streamline expansion factor $F_\star$ we obtained terminated solutions for $p > p_\star$, similar to the corresponding terminated solutions in Parker's (1958) HD wind, or, the Weber & Davis (1967) magnetized wind. For a given pressure at the Alfvén point, the requirement that a solution crosses the Alfvén and fast critical points eliminates the freedom in choosing $p_\star$ and $F_\star$ through the corresponding regularity and criticality conditions.

Table 1. Astrophysical applications for cases (a) and (b).

	Case (a)				Case (b)		
	base	Alfvén	fast	infinity	base	Alfvén	infinity
r(cm)	2×10^{11}	10^{12}	2.04×10^{12}	$\gg r_\star$	2×10^{11}	10^{12}	$\gg r_\star$
V_r(cm s^{-1})	3×10^{4}	7.7×10^{5}	1.8×10^{6}	5×10^{7}	6.5×10^{6}	3.2×10^{7}	10^{8}
B_r(G)	7×10^{-3}	5.7×10^{-4}	4×10^{-4}	10^{-3}	0.3	6.2×10^{-2}	10^{-3}
ρ(g cm^{-3})	1.6×10^{-17}	5.1×10^{-2}	1.5×10^{-2}	1.66×10^{-21}	8×10^{-18}	3.4×10^{-19}	1.66×10^{-21}
M^2	3.2×10^{-3}	1	3.34	31.3	4.22×10^{-2}	1	203
G^2	8.2×10^{-2}	1	1.41	0.477	0.206	1	64

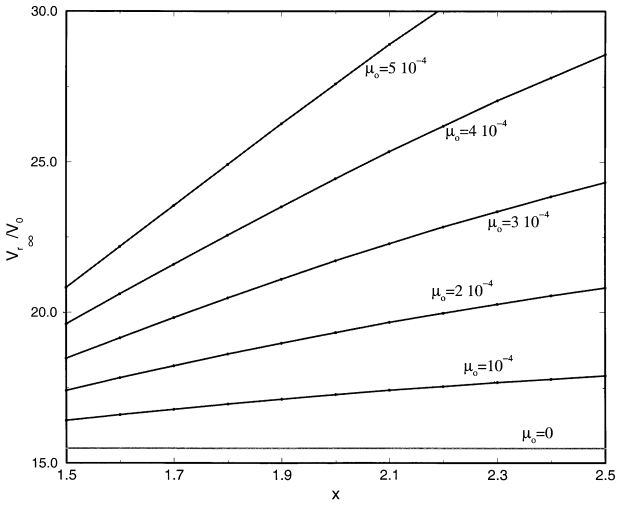

Figure 14. Dimensionless asymptotic values of the radial velocity as a function of the radiative force parameters x and μ_0 for case (b) with parameters: $\epsilon = 0.5$, $\xi = -5$, $\delta\nu^2 = 4$, $\delta_0\nu^2 = 0.001$, $\nu^2 = 0.3$, $F_\star = 1$ and $p_\star = 2$. In all these cases at the surface of the star $M_0^2 = 4.22\times10^{-2}$.

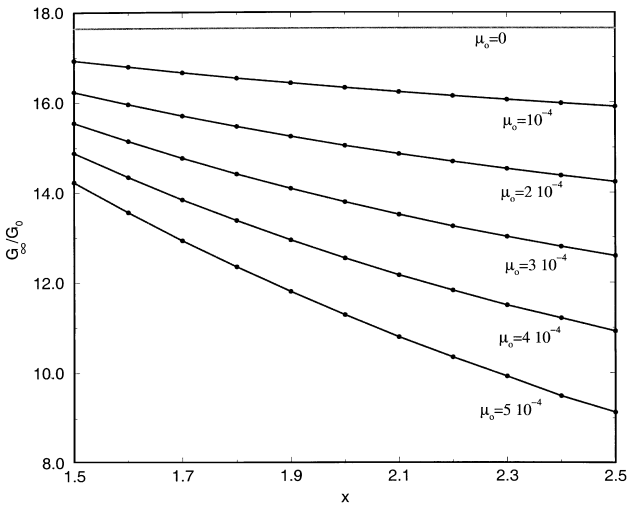

Figure 15. Dimensionless asymptotic values of the radius of the jet as a function of the radiative force parameters x and μ_0 for case (b). The other parameters are the same as in the previous figure.

A plotting of the various forces acting along and perpendicular to the poloidal streamlines reveals that the wrapping of the field lines around the symmetry axis is caused predominantly by the hoop stress of the magnetic field and is already strong at the Alfvén (and fast) critical surface. Asymptotically the cylindrical column is confined by the interplay of the inwards magnetic pinching force, the outwards centrifugal force and the pressure gradient, as in Trussoni et al. (1997). On the other hand, the acceleration of the plasma along the poloidal magnetic lines, in the near zone close to the Alfvén distance, is due to the combination of thermal pressure and magnetic forces, while at the intermediate zone beyond the Alfvén point it is basically the pressure gradient that is responsible for the acceleration.

ACKNOWLEDGMENTS

This research has been supported in part by a grant from the General Secretariat of Research and Technology of Greece. We thank J. Contopoulos, C. Sauty, G. Surlantzis and E. Trussoni for helpful discussions.

REFERENCES

Biretta T., 1996, in Tsinganos K., ed., Solar and Astrophysical MHD Flows. Kluwer, Dordrecht, p. 357
Blandford R. D., Payne D. G., 1982, MNRAS, 199, 883 (BP82)
Bogovalov S. V., 1996, MNRAS, 280, 39
Bogovalov S., Tsinganos K., 1999, MNRAS, 305, 211
Cao X., Spruit H. C., 1994, A&A, 287, 60
Chen H., Marlborough J. M., 1994, ApJ, 427, 1005
Contopoulos J., Lovelace R. V. E., 1994, ApJ, 429, 139
Ferrari A., Massaglia S., Bodo G., Rossi P., 1996, in Tsinganos K., ed., Solar and Astrophysical MHD Flows. Kluwer, Dordrecht, p. 607
Ghosh P., Lamb F. K., 1979, ApJ, 234, 296
Goodson A. P., Winglee R. M., Bohm K. H., 1997, ApJ, 489, 199
Heyvaerts J., Norman C. A., 1989, ApJ, 347, 1055
Kahabka P., Trumper J., 1996, in Van den Heuvel E. P. J., van Paradijs J., eds, Compact Stars in Binaries. Kluwer, Dordrecht, p. 425
Kakouris A., Moussas X., 1997, A&A, 324, 1071
Kudoh T., Shibata K., 1997, ApJ, 474, 362
Lamers H. J. G. L. M., 1986, A&A, 159, 90
Livio M., 1997, in Wickramasinghe D. T., Ferrario L., Bicknel G. V., eds, Accretion Phenomena and Related Outflows. Astron. Soc. Pac., San Francisco, p. 845
Low B. C., Tsinganos K., 1986, ApJ, 302, 163
Mirabel I. F., Rodriguez L. F., 1996, in Tsinganos K., ed., Solar and Astrophysical MHD Flows. Kluwer, Dordrecht, p. 683
Ostriker E. C., 1997, ApJ, 486, 291
Ouyed R., Pudritz R. E., 1997a, ApJ, 482, 712
Ouyed R., Pudritz R. E., 1997b, ApJ, 484, 794
Parker E. N., 1958, ApJ, 128, 664
Ray T. P., 1996, in Tsinganos K., ed., Solar and Astrophysical MHD Flows. Kluwer, Dordrecht, p. 539
Ray T. P., Mundt R., Dyson J. E., Falle S. A. E., Raga A., 1996, ApJ, 468, L103
Sakurai T., 1985, A&A, 152, 121
Sauty C., Tsinganos K., 1994, A&A, 287, 893
Shahbaz T., Livio M., Southwell K. A., Charles P. A., 1997, ApJ, 484, L59

Trussoni E., Tsinganos K., Sauty C., 1997, A&A, 325, 1099
Tsinganos K. C., 1982, ApJ, 252, 775
Tsinganos K., Trussoni E., Sauty C., 1992, in Schmelz J. T., Brown J., eds, The Sun: A Laboratory for Astrophysics. Kluwer, Dordrecht, p. 349
Tsinganos K., Sauty C., Surlantzis G., Trussoni E., Contopoulos J., 1996, MNRAS, 283, 811
Uchida Y., Shibata K., 1985, PASJ, 37, 515
Ustyugova G. V., Koldoba A. V., Romanova M. M., Chechetkin V. M., Lovelace R. V. E., 1999, ApJ, in press
Vlahakis N., Tsinganos K., 1997, MNRAS, 292, 591 (VT97)
Vlahakis N., Tsinganos K., 1998, MNRAS, 298, 777 (VT98)
Weber E. J., Davis L. J., 1967, ApJ, 148, 217

APPENDIX A: FUNCTIONS OF R

$$F = 2 - R\frac{G^{2'}}{G^2} \equiv \frac{\partial \ln \alpha(R,\theta)}{\partial \ln R}\,. \tag{A1}$$

$$f_1 = -\frac{1}{G^4}\,, \tag{A2}$$

$$f_2 = -\frac{F^2-4}{4G^2R^2}\,, \tag{A3}$$

$$f_3 = -\frac{1}{G^2}\left(\frac{1-G^2}{1-M^2}\right)^2\,, \tag{A4}$$

$$f_4 = \frac{F}{2RG^2}M^{2'} - \frac{1-M^2}{2RG^2}F' - \frac{\left(1-M^2\right)F(F-2)}{4R^2G^2}\,, \tag{A5}$$

with

$$F' = \frac{F}{1-M^2}M^{2'} - \frac{F(F-2)}{2R} - \frac{2RG^2}{1-M^2}f_4\,, \tag{A6}$$

$$f_5 = \frac{G^4-M^2}{G^2M^2\left(1-M^2\right)}\,, \tag{A7}$$

$$f_6 = -\frac{2}{G^4}M^{2'} + \frac{2\left(1-M^2\right)(F-2)}{RG^4}\,, \tag{A8}$$

$$f_7 = \frac{2}{R^2G^2}M^{2'} - \frac{\left(1-M^2\right)(F-2)(F+4)}{2R^3G^2} - \frac{F}{R}f_4\,, \tag{A9}$$

$$f_8 = -\frac{F-2}{R}f_5\,, \tag{A10}$$

$$f_9 = \frac{2}{M^2}\left(Q - \frac{\nu^2}{2R^2}\right). \tag{A11}$$

APPENDIX B: PHYSICAL QUANTITIES AND DIFFERENTIAL EQUATIONS OF MODEL

The MHD integrals have the following forms,

$$\Psi_A = \sqrt{4\pi\rho_\star\left(1+\delta\alpha+\mu\delta_0\alpha^\epsilon\right)}\,, \tag{B1}$$

$$\Omega = \frac{V_\star}{r_\star}\sqrt{\frac{\mu\alpha^{\epsilon-1}+\xi}{1+\delta\alpha+\mu\delta_0\alpha^\epsilon}}\,, \tag{B2}$$

$$L = V_\star r_\star\sqrt{\frac{\mu\alpha^{\epsilon+1}+\xi\alpha^2}{1+\delta\alpha+\mu\delta_0\alpha^\epsilon}}\,. \tag{B3}$$

The three ordinary differential equations for the functions of R are

$$\left.\begin{array}{c} f_0' - f_6 - f_9 = 0 \\ f_4' - f_7 + \xi\left(f_5' - f_8\right) - \delta f_9 = 0 \\ \mu\left(\frac{f_5'}{\epsilon} - f_8 - \delta_0 f_9\right) = 0 \end{array}\right\} \tag{B4}$$

or using the definitions of $P_0\,, P_1$ and F

$$\frac{\mathrm{d}G^2}{\mathrm{d}R} = -\frac{F-2}{R}G^2\,, \tag{B5}$$

$$\frac{\mathrm{d}F}{\mathrm{d}R} = \frac{F}{1-M^2}\frac{\mathrm{d}M^2}{\mathrm{d}R} - \frac{F(F-2)}{2R} - \frac{F^2-4}{2R\left(1-M^2\right)} - \frac{2G^2RP_1}{1-M^2} - \frac{2\xi R}{M^2\left(1-M^2\right)^3}\left[\left(2M^2-1\right)G^4 - M^4 + 2M^2\left(1-G^2\right)\right], \tag{B6}$$

$$\frac{\mathrm{d}M^2}{\mathrm{d}R} = \frac{M^2\left(1-M^2\right)}{\left(2M^2-1\right)G^4 - M^4}\left\{2\epsilon\delta_0G^2\left(1-M^2\right)\left(Q - \frac{\nu^2}{2R^2}\right) + \frac{F-2}{R}\left[(\epsilon+1)M^2 - (\epsilon-1)G^4\right]\right\}, \tag{B7}$$

$$\frac{\mathrm{d}P_1}{\mathrm{d}R} = -\left[\frac{F^2-4}{2R^2G^2} + 2\xi\frac{\left(1-G^2\right)^2}{G^2\left(1-M^2\right)^3}\right]\frac{\mathrm{d}M^2}{\mathrm{d}R} - \frac{M^2F}{2R^2G^2}\frac{\mathrm{d}F}{\mathrm{d}R} + \frac{2\delta}{M^2}\left(Q - \frac{\nu^2}{2R^2}\right) - \frac{M^2\left(F^2-4\right)(F-4)}{4R^3G^2} + \xi\frac{(F-2)\left[\left(2M^2-1\right)G^4 - M^4\right]}{RG^2M^2\left(1-M^2\right)^2}, \tag{B8}$$

$$\frac{\mathrm{d}P_0}{\mathrm{d}R} = -\frac{2}{G^4}\frac{\mathrm{d}M^2}{\mathrm{d}R} + \frac{2}{M^2}\left(Q - \frac{\nu^2}{2R^2}\right) - \frac{2M^2(F-2)}{RG^4}. \tag{B9}$$

The pressure component $P_2(R)$ is given explicitly in terms of the other variables:

$$P_2 = \frac{\mu}{G^2}\left[\frac{G^4-M^2}{\epsilon M^2\left(1-M^2\right)} - \left(\frac{1-G^2}{1-M^2}\right)^2\right]. \tag{B10}$$

The functional form of the pressure, equation (27), corresponds to the following functional form for the heating function:

$$\frac{q}{\rho V_{\mathrm{r}}} = \frac{V_\star^2}{2r_\star}\frac{\mathcal{Q}_0 + \mathcal{Q}_1\alpha + \mathcal{Q}_2\alpha^\epsilon}{1+\delta\alpha+\mu\delta_0\alpha^\epsilon} \tag{B11}$$

with $\mathcal{Q}_i = M^{-2(\Gamma-1)}\dfrac{\mathrm{d}}{\mathrm{d}R}\left(\dfrac{M^{2\Gamma}P_i}{\Gamma-1}\right), i = 0,1,2$. As discussed in Section 2.1, one could proceed in the reverse way, i.e. start with the functional form of the heating function and deduce the functional form of the pressure equation (27).

This paper has been typeset from a TEX/LATEX file prepared by the author.